Hierarchic random nanosphere model for broadband solar energy absorbers

Shun Cao,[1, 2] Taisheng Wang,[1] Jingli Zhao, [1] Furui Tan, [3] Xuming Zhang,[3] and Weixing Yu[4, *]

[1]*State Key Laboratory of Applied Optics, Changchun Institute of Optics, Fine Mechanics & Physics, Chinese Academy of Sciences, No.3888, Dongnanhu Road, Changchun, Jilin, China*
[2]*University of the Chinese Academy of Sciences, Beijing, 10039, China*
[3]*Department of Applied Physics, Hong Kong Polytechnic University, Hung Hom, Kowloon, Hong Kong*
[4]*Institute of Micro and Nano Optics, Key Laboratory of Optoelectronic Devices and Systems of Ministry of Education and Guangdong Province, College of Optoelectronic Engineering, Shenzhen University, Shenzhen, 518060, China*
**yuwx@szu.edu.cn*

Abstract: In this paper, a light absorbing model based on the hierarchic structure with randomly distributed nanospheres is proposed for strong absorption over 400-900 nm. The effect of different parameters including the size range, the particle number and the hierarchic height of the nanospheres on the light absorption is systematically analyzed. It is found that this structure can absorb light efficiently with an average absorptivity of 91% at the 400-900 nm waveband. The great enhancement of light absorption can be attributed to the localized surface plasmon resonant of the random metallic nanospheres as well as the strong light scattering of the metallic nanospheres embedded in the dielectric film.

OCIS codes: (260.5740) Resonance; (300.1030) Absorption; (310.6628) Subwavelength structures, nanostructures; (350.6050) Solar energy.

References and links

1. C. F. Guo, T. Sun, F. Cao, Q. Liu, and Z. Ren, "Metallic nanostructures for light trapping in energy-harvesting devices," Light Sci. Appl. **3**(4), e161 (2014).
2. R. L. Chern, Y. T. Chen, and H. Y. Lin, "Anomalous optical absorption in metallic gratings with subwavelength slits," Opt. Express **18**(19), 19510–19521 (2010).
3. K. Aydin, V. E. Ferry, R. M. Briggs, and H. A. Atwater, "Broadband polarization-independent resonant light absorption using ultrathin plasmonic super absorbers," Nat. Commun. **2**, 517 (2011).
4. Q. Liang, T. Wang, Z. Lu, Q. Sun, Y. Fu, and W. Yu, "Metamaterial-based two dimensional plasmonic subwavelength structures offer the broadest waveband light harvesting," Adv. Opt. Mater. **1**(1), 43–49 (2013).
5. S. Cao, W. Yu, T. Wang, Z. Xu, C. Wang, Y. Fu, and Y. Liu, "Two-dimensional subwavelength meta-nanopillar array for efficient visible light absorption," Appl. Phys. Lett. **102**(16), 161109 (2013).
6. S. Cao, W. Yu, T. Wang, H. Shen, X. Han, W. Xu, and X. Zhang, "Meta-microwindmill structure with multiple absorption peaks for the detection of ketamine and amphetamine type stimulants in terahertz domain," Opt. Mater. Express **4**(9), 1876–1884 (2014).
7. J. Yang, F. Luo, T. S. Kao, X. Li, G. W. Ho, J. Teng, X. Luo, and M. Hong, "Design and fabrication of broadband ultralow reflectivity black Si surfaces by laser micro/nanoprocessing," Light Sci. Appl. **3**(7), e185 (2014).
8. H. A. Atwater and A. Polman, "Plasmonics for improved photovoltaic devices," Nat. Mater. **9**(3), 205–213 (2010).
9. K. R. Catchpole and A. Polman, "Design principles for particle plasmon enhanced solar cells," Appl. Phys. Lett. **93**(19), 191113 (2008).
10. A. Ji, R. P. Sharma, A. Kumari, and N. K. Pathak, "Numerical simulation of solar cell plasmonics for small and large metal nano clusters using discrete dipole approximation," Plasmonics **9**(2), 291–297 (2014).
11. Y. Nishijima, L. Rosa, and S. Juodkazis, "Surface plasmon resonances in periodic and random patterns of gold nano-disks for broadband light harvesting," Opt. Express **20**(10), 11466–11477 (2012).
12. A. Paris, A. Vaccari, A. C. Lesina, E. Serra, and L. Calliari, "Plasmonic scattering by metal nanoparticles for solar cell," Plasmonics **7**(3), 525–534 (2012).
13. M. A. Nazirzadeh, F. B. Atar, B. B. Turgut, and A. K. Okyay, "Random sized plasmonic nanoantennas on Silicon for low-cost broad-band near-infrared photodetection," Sci. Rep. **4**, 7103 (2014).

#250632 Received 23 Sep 2015; revised 19 Oct 2015; accepted 23 Oct 2015; published 5 Nov 2015

14. A. J. Frank, N. Kopidakis, and J. Lagemaat, "Electrons in nanostructured TiO_2 solar cells: transport, recombination and photovoltaic properties," Coord. Chem. Rev. **248**, 1165–1179 (2004).
15. W. Shao, F. Gu, L. Gai, and C. Li, "Planar scattering from hierarchical anatase TiO_2 nanoplates with variable shells to improve light harvesting in dye-sensitized solar cells," Chem. Commun. (Camb.) **47**(17), 5046–5048 (2011).
16. G. K. Mor, K. Shankar, M. Paulose, O. K. Varghese, and C. A. Grimes, "Use of highly-ordered TiO_2 nanotube arrays in dye-sensitized solar cells," Nano Lett. **6**(2), 215–218 (2006).
17. C. Zha, L. Shen, X. Zhang, Y. Wang, B. A. Korgel, A. Gupta, and N. Bao, "Double-sided brush-shaped TiO_2 nanostructure assemblies with highly ordered nanowires for dye-sensitized solar cells," ACS Appl. Mater. Interfaces **6**(1), 122–129 (2014).
18. M. Torrell, R. Kabir, L. Cunha, M. I. Vasilevskiy, F. Vaz, A. Cavaleiro, E. Alves, and N. P. Barradas, "Tuning of the surface plasmon resonance in TiO2/Au thin films grown by magnetron sputtering: The effect of thermal annealing," J. Appl. Phys. **109**(7), 074310 (2011).
19. D. Buso, J. Pacifico, A. Martucci, and P. Mulvaney, "Gold-Nanoparticle-Doped TiO_2 Semiconductor Thin Films: Optical Characterization," Adv. Funct. Mater. **17**(3), 347–354 (2007).
20. Z. Zhan, J. An, H. Zhang, R. V. Hansen, and L. Zheng, "Three-dimensional plasmonic photoanodes based on Au-embedded $TiO_{(2)}$ structures for enhanced visible-light water splitting," ACS Appl. Mater. Interfaces **6**(2), 1139–1144 (2014).
21. L. Yang, X. Li, X. Tuo, T. T. V. Nguyen, X. Luo, and M. Hong, "Alloy nanoparticle plasmon resonance for enhancing broadband antireflection of laser-textured silicon surfaces," Opt. Express **22**, A577–A588 (2014).
22. H. Wang and Z. Guo, "Hierarchical TiO_2 submicron-sized spheres for enhanced power conversion efficiency in dye-sensitized solar cells," Mater. Res. Bull. **70**, 928–934 (2015).
23. I. G. Yu, Y. J. Kim, H. J. Kim, C. Lee, and W. I. Lee, "Size-dependent light-scattering effects of nanoporous TiO_2 spheres in dye-sensitized solar cells," J. Mater. Chem. **21**(2), 532–538 (2011).
24. *Lumerical lnc., "BSDF"* http://docs.lumerical.com/en/index.html?particle_scattering_bsdf.html
25. M. Langlais, J. P. Hugonin, M. Besbes, and P. B. Abdallah, "Cooperative electromagnetic interactions between nanoparticles for solar energy harvesting," Opt. Express **19**, A657–A663 (2011).
26. X. Zhang, Y. L. Chen, R.-S. Liu, and D. P. Tsai, "Plasmonic photocatalysis," Rep. Prog. Phys. **76**(4), 046401 (2013).
27. P. Zijlstra and M. Orrit, "Single metal nanoparticles: optical detection, spectroscopy and applications," Rep. Prog. Phys. **74**(10), 106401 (2011).
28. B. P. Rand, P. Peumans, and S. R. Forrest, "Long-range absorption enhancement in organic tandem thin-film solar cells containing silver nanoclusters," J. Appl. Phys. **96**(12), 7519–7526 (2004).
29. Y. Cao, P. Du, Y. Qiao, Z. Liu, and Z. Sun, "Light absorption enhancement of 100nm thick poly(3-hexylthiophene) thin-film by embedding silver nanoparticles," Appl. Phys. Lett. **105**(15), 153902 (2014).
30. Q. Fu and W. Sun, "Mie theory for light scattering by a spherical particle in an absorbing medium," Appl. Opt. **40**(9), 1354–1361 (2001).
31. I. W. Sudiarta and P. Chylek, "Mie-scattering formalism for spherical particles embedded in an absorbing medium," J. Opt. Soc. Am. A **18**(6), 1275–1278 (2001).
32. J. Y. Lee and P. Peumans, "The origin of enhanced optical absorption in solar cells with metal nanoparticles embedded in the active layer," Opt. Express **18**(10), 10078–10087 (2010).
33. B. J. Wiley, S. H. Im, Z. Y. Li, J. McLellan, A. Siekkinen, and Y. Xia, "Maneuvering the surface plasmon resonance of silver nanostructures through shape-controlled synthesis," J. Phys. Chem. B **110**(32), 15666–15675 (2006).
34. U. Kreibig and M. Vollmer, *Optical Properties of Metal Clusters* (Springer, 1995), Ch. 2.

1. Introduction

As an abundant and environmentally friendly renewable energy, solar energy has recently attracted great attentions of researchers to develop highly efficient photovoltaic devices [1]. In order to improve the efficiency, various methods have been explored, such as gratings, metamaterials and nanoparticles. Among them, periodic grating-like structures have been proved to yield high absorption with a broad waveband over a rather wide angle region [2,3]. Moreover, they are insensitive to the light polarization. For instance, K. Aydin *et al.* reported a kind of ultrathin light absorbers based on metallic gratings and trapezoid arrays with an average broadband absorption of 71% over the entire visible spectrum (400-700 nm) [3]. Our group also proposed a variety of metamaterials based absorbers, which show surprisingly high absorptive property from visible to terahertz waveband [4–6]. However, all these structures are based on the periodic nanostructure and require challenging and costly nanofabrication processes, like electron beam lithography and focused ion beam lithography. Alternatively, J. Yang *et al.* reported laser micro/nanoprocess to create surface patterns over large areas in a short time, providing a cost effective solution [7]. Also, a lot of efforts have been made to

#250632 Received 23 Sep 2015; revised 19 Oct 2015; accepted 23 Oct 2015; published 5 Nov 2015

achieve the efficient light absorbers by using the randomly sized noble metallic nanoparticles [8–13]. In comparison to the expensive nanofabrication methods, random metallic nanoparticles can be easily fabricated at a large area with much lower cost. Y. Nishijima *et al.* demonstrated that the randomly distributed Au nano-disks have an efficient broadband light harvesting effect [11]. Random sized nanoparticles were also used as plasmonic nanoantennas for low-cost broadband near-infrared photodetection on silicon [13]. In theory, both analytical method (e.g., discrete dipole approximation, DDA) and numerical computation method were used for the analysis of the light absorbing and scattering effect of the nanoparticles with different geometries [10,12]. However, all these studies made use of only a single layer of metallic nanoparticles with the same size. Till now, there is still no report on the model of hierarchic nanoparticle structures for light absorption.

In this work, a numerical model incorporated with random nanospheres was established for the analysis of hierarchic nanoparticle structure based solar energy absorbers. The hierarchic structure consists of Au-TiO_2-Au three layers and has an efficient light absorbing effect at a broad waveband from 400 to 900 nm. As one of the most important photoelectrode materials, TiO_2 nanostructures have been widely used in dye-sensitized solar cell [14]. Different morphologies of TiO_2 nanomaterials, such as nanoplates [15], nanotubes [16], and nanowires [17], have been used to increase the conversion efficiency of solar cells. In order to achieve broadband light harvesting, hierarchic Au nanospheres with different radii are introduced on the top and underneath of the TiO_2 film to form a sandwich structure. It is found that this structure can achieve an average absorption of >90% over the entire working waveband. By employing the finite-difference time-domain (FDTD) method, we proved the effectiveness of the hierarchic model and investigated the absorbing mechanisms as well.

2. Structures description and simulations setup

In the nanofabrication, it is found that the interface between TiO_2 and Au film often becomes very rough after annealing at a high temperature [18–20]. M. Torrell *et al.* observed the random distribution phenomenon of the metallic nanoparticles in the vacuum deposited TiO_2/Au films after annealing at temperature of higher than 500°C. It was shown that the initially small atomic Au clusters coalesce into separated nanoparticles under higher annealing temperature [18]. D. Buso *et al.* analyzed the film topography of TiO_2/Au film annealed at temperatures from 100 to 500°C by atomic force microscopy (AFM). It was found that the interface between TiO_2 and Au becomes quite rough after annealing [19]. Z. Zhan *et al.* showed the SEM cross-section of the Au-TiO_2 film after the thermal annealing at 600°C for 1 hour and found that the interface of the TiO_2 and Au film is rather rough and the film has actually been converted into nanoparticles [20]. Based on the above findings and to reflect the reality of experiments, this work introduced randomly distributed hierarchic nanospheres with different radii to the interface of TiO_2 and Au films, instead of a planar thin film. In order to compare the effect of random nanospheres on the improvement of light absorption, this work set up three different models in the commercial FDTD software package (Lumerical FDTD Solutions). The correlation between particle size and density of the metallic particles is considered by using the Gaussian random distribution structure group in the models, where both the size range and the number of the particles can be tuned. The Gaussian distribution property of the metallic particles after annealing is demonstrated elsewhere [20,21]. Since the distribution space in the model is fixed, larger number of particles will result in higher density and smaller number of particles means the density is lower. And the sizes of the TiO_2 particles can be controlled by tuning the parameters of the chemical process. H. Wang *et al.* obtained the typical TiO_2 spheres by a facile solvothermal process [22]. In their method, different sizes of TiO_2 nanospheres can be obtained under various conditions by changing the contents of EDA and the reaction time in the similar procedures. In addition, I. G. Yu *et al.* demonstrated another method to control the sizes of TiO_2 spheres in the preparation of nanoporous TiO_2

#250632 Received 23 Sep 2015; revised 19 Oct 2015; accepted 23 Oct 2015; published 5 Nov 2015

spheres [23]. They simply adjusted the titanium tetraisopropoxide/H_2O molar ratio (r-factor) to form different size of TiO_2 nanospheres.

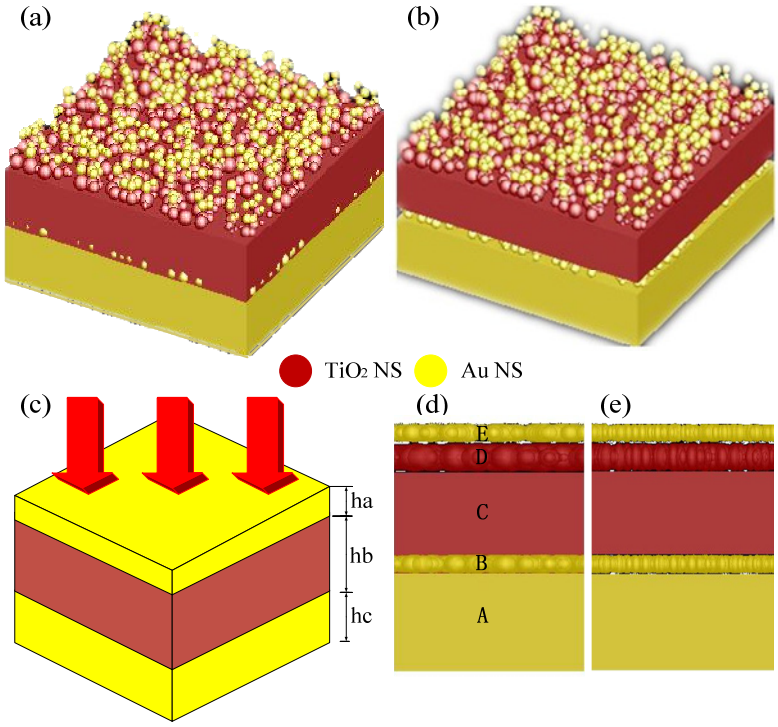

Fig. 1. Schematics of the proposed three models of solar energy absorbers: (a) perspective view and (d) cross-sectional view in the *xz* plane ($y = 0$) of Structure 1, (b) perspective view and (e) cross-sectional view in the *xz* plane ($y = 0$) of Structure 2, and (c) perspective view of Structure 3.

Figure 1 shows the schematic diagrams of the proposed models for solar energy absorbers. Structure 1 (in short, S1) is the absorber that could realize light harvesting using an effective absorbing layer. Figures 1(a) and 1(d) show the perspective and cross-sectional views in the *xz* plane ($y = 0$) of S1. The absorber consists of five layers: two Au random particle layers, a TiO_2 random particle layer, an Au film and a TiO_2 film. The red spheres stand for TiO_2 nanospheres (NSs) and the yellow ones stand for Au NSs. *Layer A* denotes the Au film with a thickness of 200 nm; *Layer B* represents the layer of Au random spheres, which have the radii ranging from 20 to 40 nm and are tightly distributed in a 1 μm × 1 μm × 40 nm space. From Fig. 1(d), it is seen that Layer B acts as the effective medium layer. *Layer C* is a layer of pure TiO_2 film and has no Au NSs, its thickness is 170 nm. Further up, *Layer D* contains 800 TiO_2 random spheres. The radii of these particles range from 10 to 60 nm. The sizes and numbers of nanospheres in Layer B and Layer D are meant to represent the roughness of the interface. Lager sizes and larger numbers indicate higher roughness of the interface. On the top, *Layer E* is a layer of random Au particles, whose radius varies from 20 to 40 nm. The total number is 400, and the particles are allowed to overlap with each other. Structure 2 (S2) depicted in Figs. 1(b) and 1(e) is similar to S1 but has no effective medium in Layer B, i.e. without TiO_2 nanospheres filling the remaining space. Figure 1(c) shows the perspective view of Structure 3 (S3). It consists of three films (i.e., Au-TiO_2-Au films) and does not have any random nanospheres. The thicknesses of the top Au film, the central TiO_2 film and the bottom Au film are $h_a = 60$ nm, $h_b = 230$ nm and $h_c = 240$ nm, respectively.

#250632 Received 23 Sep 2015; revised 19 Oct 2015; accepted 23 Oct 2015; published 5 Nov 2015

Three structures were analyzed in the software. The three-dimensional simulations were performed with a plane wave source incident in the z direction. Periodic boundary conditions were employed for both the x and y directions and Perfect Match Layer (PML) boundary condition was employed in the z direction. Since the distribution of the random particles is non-periodic, the periods of the unit cell in both the x and y directions were set as 1000 nm, which is far greater than the radius of the random particles. Under this condition, one can simulate the rough surface with a good approximation to the real case [24]. The high accuracy mesh type, i.e. the 6th level of the auto non-uniform mesh type, was used to ensure a reliable result. The absorptivity was calculated by using the equation $A(\lambda) = 1\text{-}R(\lambda)\text{-}T(\lambda)$, where $R(\lambda) = |S_{11}|^2$ is the reflection and $T(\lambda) = |S_{21}|^2$ is the transmission. Since the thickness of the bottom Au film (200 nm) is much larger than its typical skin depth, there is nearly no transmittance in the overall frequency range, i.e. $T(\lambda) = 0$. In this case, the formulation used to calculate the absorptivity is simplified as $A(\lambda) = 1\text{-}R(\lambda)$. Frequency-domain field and power monitor were used to investigate the S-parameters of transmission (S_{21}) and reflection (S_{11}) of a single unite cell.

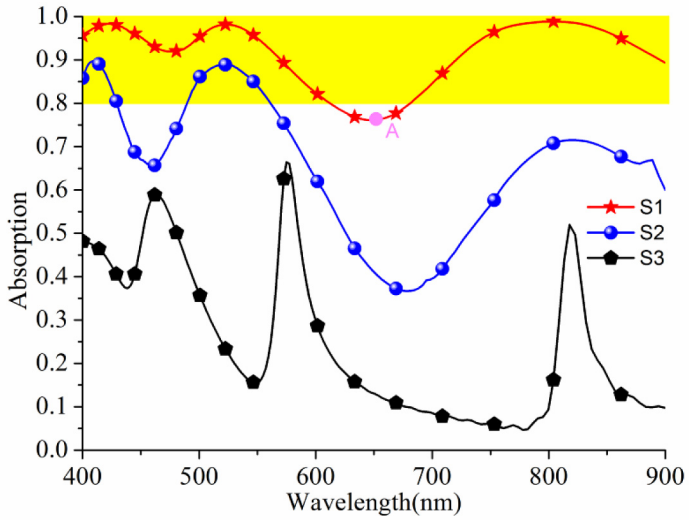

Fig. 2. Absorption spectra of three absorbers: S1 (red), S2 (blue), and S3 (black) over the waveband of 400-900 nm for the normal incident light. The yellow zone has > 80% absorption.

Figure 2 shows the absorption spectra of three structures for the normal incident light. It can be clearly seen that the absorption (the black curve) of simple Au-TiO_2-Au structure (S3) is the lowest among three structures and it has three peaks at wavelengths of 463, 574 and 817 nm, the corresponding absorptivity at these wavelengths is 58.9%, 66.3% and 52.0%, respectively. The average absorption at the entire waveband is only about 30%. However, when the random nanospheres are added into the structure, one can find that the absorption is increased significantly (see the red and blue curves in Fig. 2). In other words, random nanospheres play an important role in the increasing of the absorption of the nanostructures. Figure 2 also reveals that the effective medium layer (EML) can further enhance the absorption by comparing the red curve (corresponding to the structure S1 that has the EML) and the blue curve (corresponding to the structure S2 that has no EML). For structure S1, only the absorption over the waveband of 613 to 679 nm is lower than 80% and the minimum absorption (point A in Fig. 2) is 76.1% at 647 nm. The maximum absorption of S1 goes up to 98.8% at 804 nm. The average absorption of structure S1 at the entire waveband of 400-900 nm is larger than 90%. In comparison, the absorption of structure S2 is much lower than that of structure S1 and the average absorption at the entire waveband is only about 65%. The

#250632 Received 23 Sep 2015; revised 19 Oct 2015; accepted 23 Oct 2015; published 5 Nov 2015

maximum absorption of structure S2 is 89.2% at 406 nm and the minimum is only 36.7% at 678 nm. In summary, structure S1 has the best absorption performance in comparison to the other two structures due to the introductions of the random nanoparticles and the EML. More specifically, the average absorption is increased by 39.2% due to the random nanoparticles layer and by 61.9% further due to the EML.

3. Numerical investigation of the absorption mechanism

In order to understand the absorption mechanism of S1, the electric field distributions at different wavelengths were calculated for the *xy* planes at $z = +0.17$ (see Fig. 3), + 0.12 (Fig. 4) and –0.1 μm (Fig. 5), which correspond to the z centers of three layers of random nanospheres (i.e. Layer E, Layer D, Layer B), respectively. The wavelengths were chosen to be 474, 522, 647 and 804 nm, which correspond to the absorption maxima and minima (see the red curve in Fig. 2). The corresponding absorptions at these wavelengths are 91.9%, 98.1%, 76.1% and 98.8%, respectively.

From Figs. 3-5, one can observe clearly that the electric field hot spots are located mainly at the positions of Au and TiO_2 nanospheres, which means the electric field has been greatly enhanced at these positions. In particular, in Fig. 3, the electric filed at all wavelengths has been greatly enhanced by the Au nanospheres at the top layer (Layer E), which means that the top random Au nanospheres layer is crucial to the enhancement of absorption over the whole waveband. Apparently, this phenomenon can be attributed to the localized surface plasmon resonance (LSPR) effect [25–27]. When the light strikes on the Au nanospheres, the conduction band electrons are excited to oscillate collectively [26]. This results in the strong optical absorption and thus the conversion of the light into heat rapidly [27].

At the same time, as can be read from the scale bars in Fig. 3, the enhancement factor of the electric field becomes more pronounced for the wavelength larger than 500 nm. Especially for the wavelength 522 nm, the electric field intensity induced by the LSPR is almost doubled in comparison to that at 474 nm. For example, the maximum is only 4.5 in Fig. 3(a), but goes up to 9, 10 and 25 in Figs. 3(b)-3(d), respectively. Although the electric field enhancements in TiO_2 random NSs layer and the bottom Au NSs layer are quite weak as shown in Figs. 4 and 5, the total enhancement of the electric field at 522 nm is still rather strong so that the absorption is still as high as 98.1%. While for the TiO_2 random NSs layer (see Fig. 4), the enhancement of the electrical field becomes weaker when wavelength is larger than 522 nm and the weakest at the wavelength of 647 nm as shown in Fig. 4(c). From the Figs. 4(c) and 4(d), we can find the electric field hot spots are enhanced and TiO_2 random NSs in other position also enhance the electric distribution when the wavelength become 804 nm. Moreover, the enhancement of the electrical field by the TiO_2 random NSs is much weaker than that of the Au random NSs in *Layer E* even for shorter wavelengths as shown in Figs. 3(a) and 4(a).

As to the bottom Au NSs layer in Fig. 5, it is apparent that this layer contributes to the light absorption at the entire waveband, similar to the top Au NSs layer. However, it seems that the enhancement of the electric field is stronger as the wavelength goes longer. For instance, the maxima of scale bar are 1.7, 2.2 and 4.4 for Figs. 5(a)-5(c), but it goes up to 8 in Fig. 5(d). This might be attributed to the hierarchic structure of the bottom Au NSs in this layer. Since the sizes of the Au NSs are in the range of 20-40 nm and the Au NSs distribute densely in the cuboid with a height of 40 nm, it is possible for the NSs to partially overlap with each other. In this case, the intimately contacted small NSs might be considered to form larger nanoparticles with irregular shape (called quasi-nanoparticles). As a result, these large quasi-nanoparticles interact better with long wavelength due to the LSPR effect.

#250632 Received 23 Sep 2015; revised 19 Oct 2015; accepted 23 Oct 2015; published 5 Nov 2015

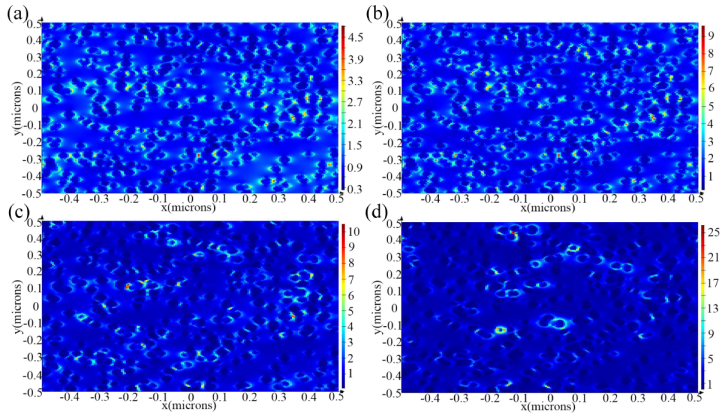

Fig. 3. Distribution of the electric field intensity of Structure 1 in the *xy* plane (z = + 0.17 μm) at four featured wavelengths. (a) 474 nm, (b) 522 nm, (c) 647 nm, and (d) 804 nm. This plane is the central plane of the top layer (i.e., the random Au nanoparticle layer, Layer E).

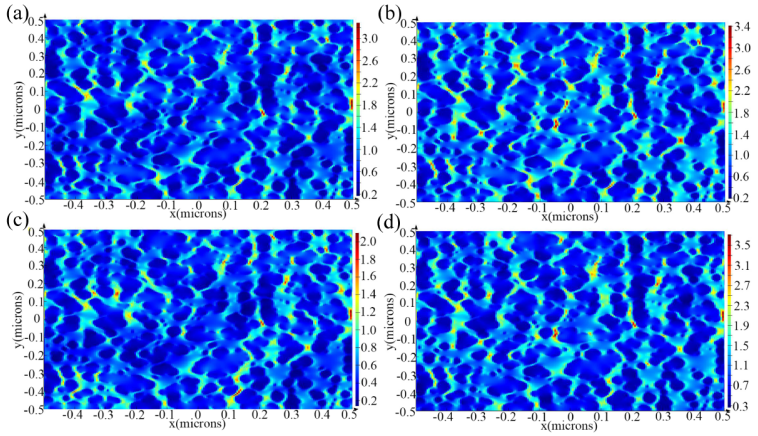

Fig. 4. Distribution of the electric field intensity of Structure 1 in the *xy* plane (z = + 0.12 μm) at four featured wavelengths. (a) 474 nm, (b) 522 nm, (c) 647 nm, and (d) 804 nm. This plane is the central plane of the random TiO_2 nanoparticle layer (i.e., Layer D).

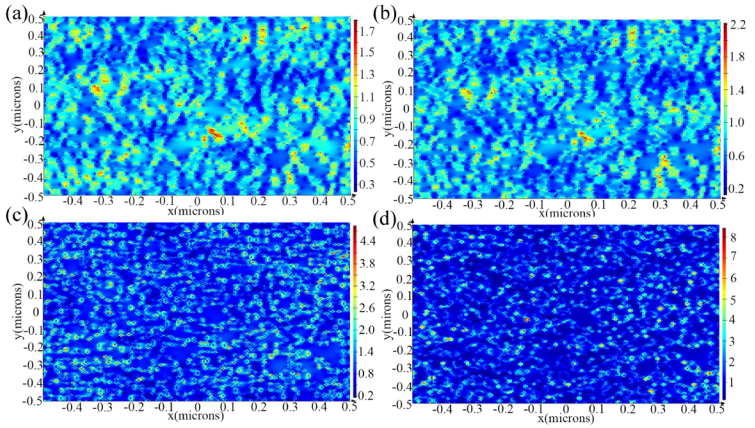

Fig. 5. Distribution of the electric field intensity of Structure 1 in the *xy* plane (z = –0.1 μm) at four featured wavelengths. (a) 474 nm, (b) 522 nm, (c) 647 nm, and (d) 804 nm. This plane is the central plane of the Au random sphere layer (i.e., Layer B).

#250632 Received 23 Sep 2015; revised 19 Oct 2015; accepted 23 Oct 2015; published 5 Nov 2015

In addition to the LSPR effect, the high absorption of structure S1 could also be attributed to the strong light scattering of the nanoparticles. Previous studies showed that embedded Ag nanoparticles could effectively increase the absorption in ultrathin organic solar cells and thereby improve the efficiency [28,29], and attributed such an improvement to the scattering and extinction induced by nanoparticles [30,31]. For instance, J. Y. Lee *et al.* used a generalized Mie approach to investigate the mechanism of optical absorption enhancement in the metallic nanoparticles embedded in the dielectric medium [32], and found that strong scattering leads to strong local optical electric fields and therefore enhanced optical absorption.

4. Effects of different nanosphere parameters on absorption

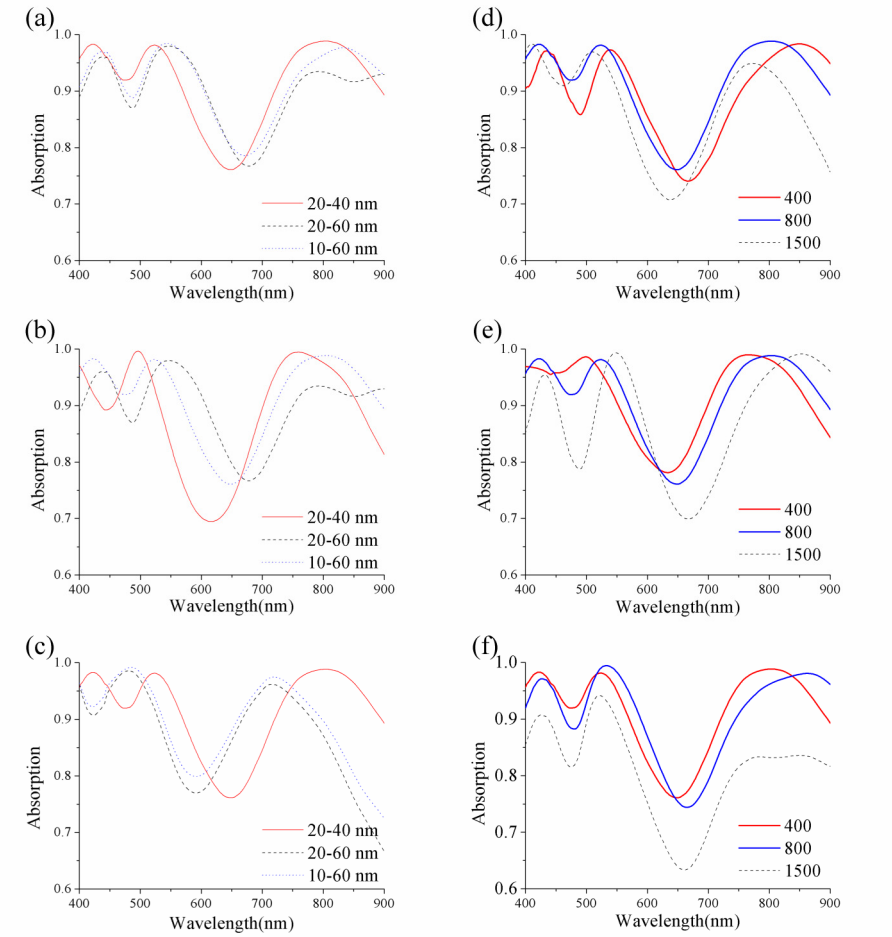

Fig. 6. Influences of the radius and the number of NSs on the absorption spectra for different layers: (a) and (d) for the top Au NSs layer (i.e., Layer E), (b) and (e) for the TiO_2 NSs layer (i.e., Layer D), (c) and (f) for the bottom Au NSs layer (i.e., Layer B), respectively.

To further understand the light absorption performance of structure S1, the effects of different parameters such as the radius and the number of nanospheres were studied. Figures 6(a)-6(c) show the absorption spectra for different radii of nanospheres in Layer E, Layer D and Layer B, respectively. In these figures, the red curve stands for the absorption of structure S1. One can find from Figs. 6(a) and 6(b) that the resonance wavelength has a red shift when the range of the Au nanosphere diameter is increased from 20 to 40 nm to 20-60 nm. In contrast, the

#250632 Received 23 Sep 2015; revised 19 Oct 2015; accepted 23 Oct 2015; published 5 Nov 2015

resonance wavelength has a blue shift when the range of the Au nanosphere diameter is broadened from 20 to 60 nm to 10-60 nm. These phenomena are consistent with the previous study using the DDA numerical calculation [33]. The effects of different shapes of nanostructure on the resonance wavelength and the electric field intensity were also calculated. Because of the restoring force of the electron oscillation, charge separation (i.e. surface polarization) plays a dominant role in determining the frequency of the plasmon resonance [34]. However, the resonance frequency shifts anomalously when the range of the radius of Au NSs in the bottom layer is varied as shown in Fig. 6(c). The absorption curve has a blue shift as the number of larger Au NSs increases and a redshift with the number of smaller Au NSs increases. These phenomena are not in agreement with the conclusion in reference [33]. Again it can be attributed to the unique hierarchic structure of the bottom layer of Au NSs. When there are more large NSs in the cuboid, the distribution of the NSs tends to be a single layer and therefore the degree of the hierarchic becomes weaker. In this case, the quasi-nanoparticles become smaller and thus the resonance of the wavelength has a blue shift. One the other hand, when there are more small NSs, the overlap between the small particles becomes stronger and thus the degree of hierarchy becomes stronger. In this case, the number and the effective size of the quasi larger nanoparticles are increased. As a result, the resonance wavelength has a red shift.

Furthermore, the effect of the number of nanospheres on the absorption was also analyzed and the results are shown in Figs. 6(d)-6(f). Figure 6(d) shows that the optimal number of the Au NSs should fall into the range of 400-800. In particular, when the number of Au NSs is 1500 (i.e. high density of Au NSs), the absorption drops dramatically, especially at the long waveband. It is because that the upper Au NSs layer can be regarded as a relatively smooth and dense Au film in this case so that much more light is reflected back to the air. The same tendency can also be found in Figs. 6(e) and 6(f), the absorption goes down with the increase of the number of NSs. From Fig. 6(e), it can be found that the resonance wavelength has a redshift with the increase of the number of TiO_2 NSs, which can be explained by the same reason mentioned above.

5. Conclusions

In summary, we have reported the design of an efficient absorber by using the random nanosphere model that can achieve over 90% absorption over 400-900 nm. In comparison to the structure of the traditional sandwich-like absorber, the random sphere model shows a great enhancement effect on the light absorption. The high absorptivity can be explained in terms of the localized surface plasmon resonance effect and the strong scattering of Au NSs embedded in the TiO_2 medium. Finally, the effects of different parameters of random nanospheres on the light absorption were also analyzed and discussed. It is found that the large range of radius distribution and the large numbers of nanospheres (i.e. dense nanospheres), are not preferable for the light absorbing.

Acknowledgments

The authors acknowledge the financial supports from Natural Science Foundation of China under grant numbers 61361166004, 61490712, 61475156 and 61377068, and from The Research Grants Council of Hong Kong under the grants N_PolyU505/13 and PolyU 5334/12E.

#250632 Received 23 Sep 2015; revised 19 Oct 2015; accepted 23 Oct 2015; published 5 Nov 2015